Novel methodologies for the characterization of airflow properties of shading screens by means of wind-tunnel experiments and CFD numerical modeling

Novel Methodologies for the characterization of airflow properties of shading screens by means of wind-tunnel experiments and CFD numerical modeling

Enrica Santolini[b], Beatrice Pulvirenti[a], Daniele Torreggiani[b], Patrizia Tassinari[b]

[a]*Department of Industrial Engineering, University of Bologna, via Terracini 34, 40131, Bologna, Italy*
[b]*Department of Agricultural and Food Sciences, University of Bologna, Via Giuseppe Fanin 48, 40127, Bologna, Italy*

Abstract

Shading screens are broadly used in the protected cultivation sector, since they allow both to reduce the heat load and thus to control temperature, and to have lower and uniform levels of light intensity inside greenhouses. Various types of shading screens are available on the market, with different colors, material and textures. The choice of the best screen depends on the specific application and needs of the grower. Despite this, some screens can negatively affect ventilation and indoor climate, since their porosity can generate extra mass, heat and momentum transfer resistance. Most studies have evaluated the screen-related parameters, such as permeability and porosity, and the screen effect on ventilation referring to screens with simple and regular textures. In this paper, these parameters have been measured for three screen types available on the market using different approaches for their characterization. A novel approach based on image analysis together with wind tunnel tests has been set up to yield the permeability and inertial coefficient. On the other hand, a computational methodology based on CFD modeling has been carried out in order to obtain the relation between air velocity through a screen and the relative pressure drop, avoiding any experiment. The CFD methodology has been developed and validated, with the aim to possibly derive the parameters of different screens through simulations rather than more demanding experiments feasible only with specific equipment. In particular, a portion of the whole screen has been chosen for CFD simulations and the numerical results have been validated by a comparison with Particle Image Velocimetry (PIV) data. This has allowed both to improve the model and to evaluate its effectiveness in simulating this specific fluid dynamics domain. By these novel approaches, the basis for extending the knowledge about the characterization of the screens used in agriculture have been laid.

Corresponding Author: enrica.santolini2@unibo.it

Keywords: Wind tunnel, Particle Image Velocimetry, CFD, Shading screens, Porosity

1. Introduction

Thanks to the development of new materials and technological advancements, a considerable number of screen types for the agricultural sector have become available on the market, and can be used depending on the specific application field. Several types of screen are commonly used in conjunction with windows or large glass patio doors to prevent insects or large bits of debris from entering a household when these windows or doors are open (Norris and Collins, 2015). In the protected cultivation sector, thermal screens are used as a cheap and effective way to reduce the night-time heat loss; shading screens are used to reduce the day-time heat load and thus to control temperature (Fabrizio, 2012), as well as to have lower and more uniform levels of light intensity inside greenhouses; insect-proof screens prevent the entrance of both insects and birds (Miguel, 1998). The use of screens in general, and in particular the application of thermal and reflective screens in greenhouses, has increased in all those countries - such as Italy and other Mediterranean countries - where uncontrolled solar radiation would remarkably affect the possibility to control light and climate inside greenhouses and thus to maintain suitable conditions for plant growth over the entire product (Castellano et al., 2009) (Vox et al., 2014). Focusing on the shading devices, the choice of the most suitable screen among the many solutions available depends on the specific application and production needs of the grower. For example, shading curtains can be placed outside of the structure, just above the roof, or inside the structure. Depending on that configuration, the screens can have different color, material and texture. Focusing on internal shading screens, due to their characteristics and location, they can negatively affect ventilation and indoor climate because they can generate extra mass, heat and momentum transfer resistances, caused by their porosity (Katsoulas et al., 2006) (Santolini et al., 2018). In particular, their low porosity can affect the ventilation, reducing air velocity and modifying the air patterns in the cultivation area, and consequently the indoor climatic conditions, increasing air temperature and humidity, and thus causing less favorable conditions for the crops. Moreover, a porous surface, as a screens, can affect the free convection heat transfert from a window glazing if placed adjacent, as studied by Naylor et al. (2017), but also the convective and radiation heat transfer through the glass into the structure, as studied by Norris and Collins (2015). The porosity of a screens is defined as the ratio of open to total area, depending on the distances between two adjacent weft and warp threads as explained in Teitel and Shklyar (1998). The majority of the case studies available in literature have been characterized by the regularity of weft and wrap threads disposition, in order to determine permeability and porosity values (Miguel et al., 1997) (Teitel, 2010) (Valera et al., 2006). Nowadays, shading screen texture presents less regular geometry and the ratio of open to total area, so as the distances between weft and warp threads, are not easily identifiable. Due to the complex texture, the porosity can not be calculated and the other parameters related to the ventilation can

not be obtained. Consequently the screens effect on the ventilation and micro-climate of a greenhouse can not be investigated. Therefore, more sophisticated systems are necessary to obtain the physical parameters driving the ventilation processes, and thus to investigate the effect of screens on ventilation and micro-climate inside greenhouses. Few studies are focused on investigating the variation of micro-climatic conditions due the presence of screens in greenhouses using a CFD approach, despite the importance of knowing which are the conditions in the cultivation area (Santolini et al., 2018). It is well known that, considering the porous media approach to estimate the screen effect, the pressure drop through a porous media, depending from the fluid velocity, is expressed by the Darcy-Forchheimer's law (Sobieski and Trykozko, 2014a) (Sobieski and Trykozko, 2014b). Those parameters, necessary to evaluate the air flow characteristics of greenhouse screens, are intrinsically related to the porosity of the surfaces. Several equations are available in the scientific literature, allowing to obtain the permeability and inertial coefficient from porosity. For example, several models can be applied for relating Y and K with the porosity of the surface, such as the ones presented in Miguel et al. (1997) and Miguel (1998). In fact, the authors considered the equation (5) as the best expression of the relationship between porosity and, respectively, permeability and inertial coefficient. These relations were obtained by testing 14 different screens. New relations could be found Flores-Velazquez and Montero (2008). Several authors have used these equations to derive the parameters necessary to perform CFD studies of greenhouses with screens (Bartzanas et al., 2002), (Campen and Bot, 2003), (Fatnassi et al., 2003), (Molina-Aiz et al., 2004), (Campen, 2005). However, several authors, such as (Teitel, 2007), have demonstrated that these relations (Eq.(5),eq.(6) and eq.(7)) could lead to an overestimation of the parameters, between 1.5 and 5 times. Therefore, further experimental trials are necessary to assess the physical parameters of screens with complex textures, and check the validity of the existing equations relating permeability and other airflow coefficients to porosity. Porosity of screens with complex textures may not be reported on technical data sheets, therefore specific methodologies are necessary to assess it accurately. Obtaining screens' properties through experimental trials can be very demanding, and calls for specific equipments. Therefore, a CFD approach can be a very useful and efficient way to simulate the airflow through the porous surface of the screens (Teitel, 2010) (Zhang et al., 2018). Teitel (2010) proposed two different approaches studying woven screens. In the first approach, the realistic models of studied screens were simulated. Moreover, in the second approach, each screen was simulated as an 8-mm thick porous slab. The study found out that the most effective way to obtain K and Y for woven screens with mono-filament threads was to consider each screen individually, rather than searching for a global correlation between K and Y and alpha, based on tests of screens with differing porosity. Nevertheless, no CFD methodology has been validated for screens with other irregular textures. Therefore, further research is necessary to define specific CFD modeling and simulation methodologies applicable to more complex textures, and

to validate them against experimental data. The general goal of this paper is to define and test both experimental and simulation methodologies, aimed to assess fluid-dynamics properties of shading screens with complex textures and their relationships, suitable to evaluate their impact on ventilation in the greenhouses cultivation field. The specific goals of this paper are as follows:

1. to estimate experimentally the airflow parameters of three types of screens available on the market, by means of an original specific methodology of wind tunnel tests;

2. to evaluate the extent to which the equations available in the scientific literature, applicable for deriving those parameters from porosity, can be applied to different types of screen textures, thanks to an original image analysis methodology, designed to obtain the porosity of screens with complex textures;

3. to develop a CFD methodology and compare it to Particle Image Velocimetry (PIV) data with the purpose of verifying the possibility to derive the shading screens parameters through CFD simulations rather than more demanding experiments to be carried out using specific equipment.

A series of methodologies have been defined in an alternative and interchangeable way for the research and definition of these specific parameters.

2. Theory

A fundamental law linking pressure drop and velocity in fluid flow through porous media is Darcy's law (1856) (eq. 1) (Sobieski and Trykozko, 2014a). This relation can be applied to flows of gases, liquids, or mixtures.

$$\frac{\Delta p}{\Delta x} = -\frac{\mu}{K} u \tag{1}$$

$$\beta = \frac{Y}{K^{\frac{1}{2}}} \tag{2}$$

where μ is fluid dynamic viscosity (Pa s), K is permeability to the fluid (m^2) of the media and u is the fluid velocity. However, the Darcy's law suitably describes the flow in porous media for low flow velocities (Reynolds number lower than 10) if the fluid can be treated as incompressible and Newtonian (Hellström and Lundtröm). When the velocity magnitude increases and so the Reynolds number, the differencies between experimental results and Darcy's low results are visible, as shown by Hellström and Lundtröm. This discrepancy has been explained by Forchheimer by adding the inertial effects; in the equation representing of kinetic energy (see eq. 3) (Sobieski and Trykozko, 2014a; Costa et al., 1998; Ewing et al.):

$$\frac{\Delta p}{\Delta x} = \frac{\mu}{K}u + \rho\beta|u|u \tag{3}$$

$$\beta = \frac{Y}{K^{\frac{1}{2}}} \tag{4}$$

where K is permeability to air (m^2), μ is air dynamic viscosity (Pa s), ρ is air density and β is non-Darcy coefficient (1/m), which in specific defined as visible in (4).
The Darcy-Forchheimer's law has been applied in the modeling and characterization of varoius types of screens, used in the agricultural sector (Miguel et al., 1997). From the equation 3, the permeability and the inertial coefficient of a porous media can be derived. In particular, in Miguel (1998) presented a model for relating Y and K with the porosity for agricultural screens:

$$K = 3.44 \times 10^{-9}\alpha^{1.6} \quad and \quad Y = 4.3 \times 10^{-2}\alpha^{-2.13} \tag{5}$$

where α is the porosity of the samples.
A similar correlation was given by Valera et al. (2005) obtained by testing eleven different screens in a wind tunnel:

$$K = 5.68 \times 10^{-8}\alpha^{3.68} \quad and \quad Y = 5.67 \times 10^{-2}\alpha^{-1.1604} \tag{6}$$

$$K = 2 \times 10^{-7}\alpha^{3.3531} \quad and \quad Y = 0.342 \times 10^{-2}\alpha^{-2.5917}. \tag{7}$$

These are the expressions frequently used for the determination of the porous media characteristics.

3. Materials and Methods

The characterization of the parameters of a screen, such as porosity and permeability, is important in order to understand how the flow through it is affected. This section describes the shading screens details and all the approaches set up and used in this study for characterizing their airflow parameters, as follows:

- screens texture;
- wind tunnel measurements for the pressure drops measurements;
- image analysis process for a screen porosity determination;
- CFD modeling and simulation of a screen and Particle Image Velocimetry (PIV) measurements used for CFD validation.

3.1. ***Screens description***

The following types of shading screens, frequently used in Northern Italy region, have been selected (Shading screens produced by Svensson Corporation):

- Harmony 4215 O FR;
- Harmony 5220 O FR;
- Harmony 3647 FR.

Those screens, hereinafter named H3, H4 and H5, respectively, are commonly used in the cultivation of various horticultural crops, including ornamental plants. These screens belong to the same family of products, and have similar characteristics in acting as a barrier to direct sunlight, and in diffusing solar light. At the same time, they show remarkable differences in terms of texture, as shown in figure 1, obtained through a high-definition scanning process.

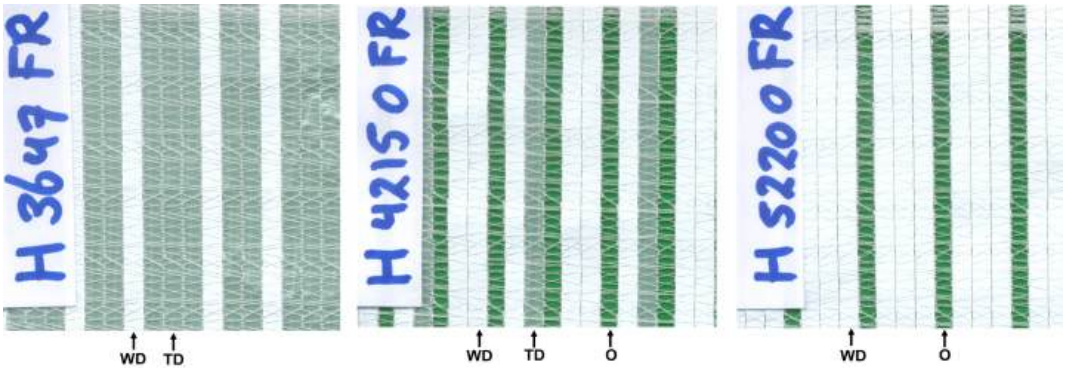

Figure 1: Picture of the three samples, made using a scanner of 1200 dpi. From left to right are shown H3, H4 and H5 and the texture characteristics are reported below.

They are three types of shading screens commonly applied in the cultivation, for strawberries, horticultural and ornamental plants. These screens belong to the same family of products and they have quite similar characteristics in terms of direct solar radiation barriers and as diffusive solar light diffusers, with slightly higher performance for H5 compared to the others, as readable from data sheets. Instead, they have significant diversities in terms of texture, as shown in figure 1 obtained through a scanning process. In fact, H3 is composed by 3 transparent diffuse (TD), 1 white diffuse (WD), 2 TD, 1 WD, of 4 mm width each. H4 is composed by a pattern of strips as 1 WD, 1 TD, 1 open, 2 WD, 1 open (O) (only the thread weft is present); H5 is composed by 3 WD, 1 O, 2 WD, 1 O stripes. The H3 is the only one without any open strip. A summary of the geometrical and optical screens characteristics are presented in table 1.

Table 1: Geometrical and optical characteristics of the three screens investigated

Screens	Texture	Geometry	Optical properties
H3647 FR		- 100 % Polyester - Weight 57 g/m^3 - Width strips 4 mm - Pattern: 3 transparent diffuse, 1 white diffuse, 2 transparent diffuse, 1 white diffuse	- Shading level in direct light, PAR 43 % - Shading level in diffused light, PAR 50 % - Energy saving 47 %
H4215 OFR		- 100 % Polyester - Weight 54 g/m^3 - Width strips 4 mm - Pattern: 2 white diffuse, 1 open, 1 white diffuse, 1 transparent diffuse, 1 open	- Shading level in direct light, PAR 48 % - Shading level in diffused light, PAR 53 % - Energy saving 15 %
H5220 OFR		- 100 % Polyester - Weight 61 g/m^3 - Width strips 4 mm - Pattern: 3 white diffuse, 1 open	- Shading level in direct light, PAR 52 % - Shading level in diffused light, PAR 52 % - Energy saving 20 %

3.2. ***Wind tunnel tests***

The experimental tests have been conducted in a wind tunnel, placed in the Fluid-dynamics and Heat Transfer laboratories of the Department of Industrial Engineering of the University of Bologna (DIN).

Figure 2: Picture of the entire wind tunnel at the Department of Industrial engineering (DIN). The test chamber and the test section have been highlighted in yellow and the fan have been highlighted in blue

.

It is a wind tunnel with a test chamber of 30 × 30 × 60 cm as dimensions. It is composed by an honeycomb of 90 cm of side, connected to a convergent channel, which is directly connected with the test section (fig. 2). After the test chamber, there is a divergent channel connected to a rectangular test section, which leads to the fan, end of the system. In specific, in this system, the fan has a diameter of 45 cm and can reach limit frequency of 50 Hz. In the apparatus, the tests have been conducted with the goal of evaluating the parameters K, Y and β of the three screens. Before starting the experiments, in order to obtain the relation between the frequency of the fan and the velocity of the fluid, the calibration curve of the system has been determined.

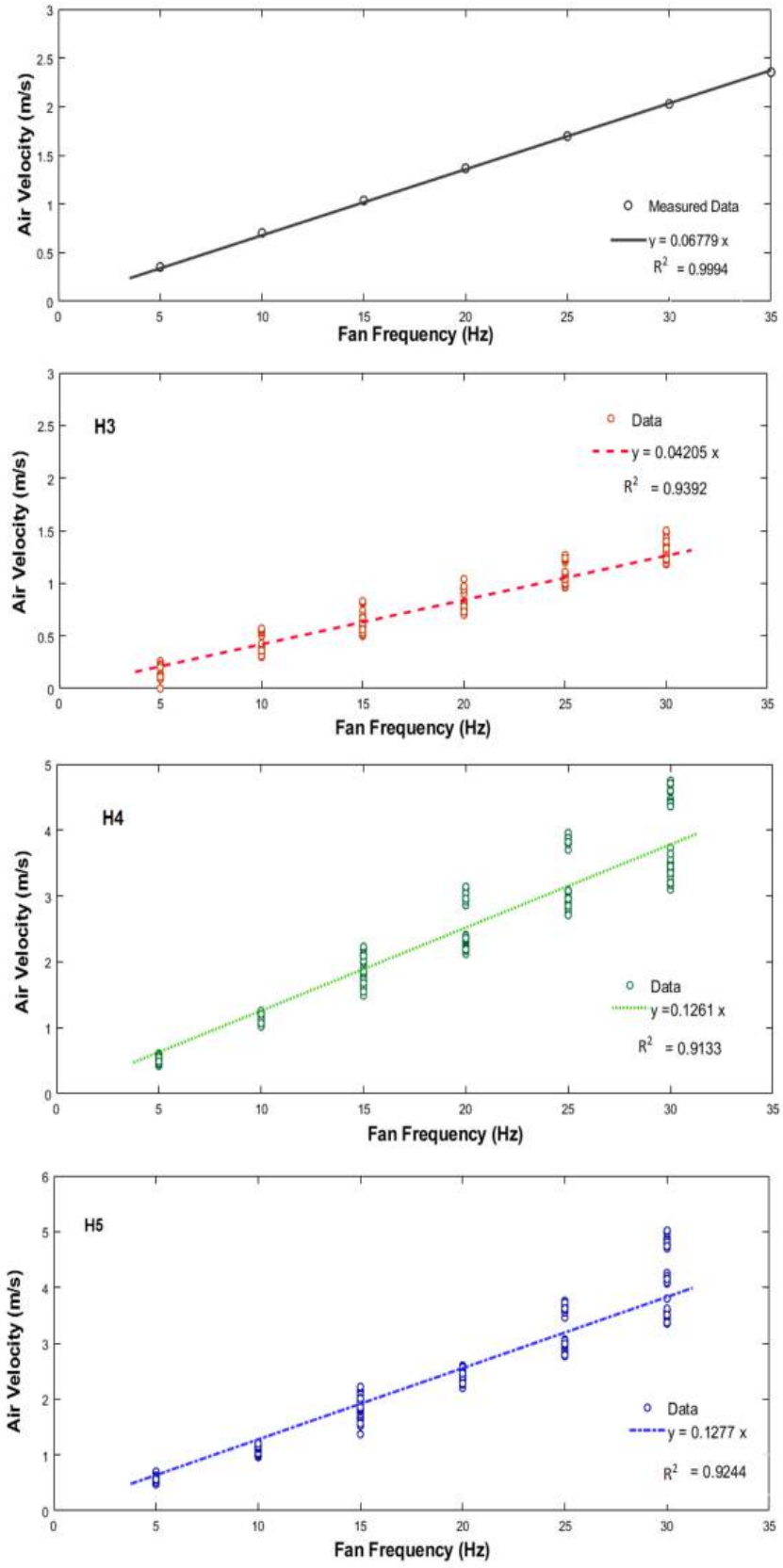

Figure 3: Calibration curves of different cases, from up to bottom: calibration curve of the wind tunnel, calibration curve of the case with screen H4215, the one for the case of screen H5220 and finally the on of screen H3647.

First of all, the wind tunnel has been characterized by collecting velocities data in three different positions along the width of the test chamber, precisely 3 cm from both walls and in the middle of the section, with a Pitot probe and a micro-manometer with a sensibility of 0.01 m/s (Model 8710 DP-Calc Micromanometer). The data were collected for 30 seconds, repeated for four times in each position. These measurements have been performed for different fan frequencies, starting from 5 Hz to 30 Hz. The same type of measurements have been reproduced in presence of each screen sample. A sample of 30 $\times$ 30 cm of dimension has been prepared, for each screen, with a frame as support during tests. In these cases, the instrument has been placed distant from the screen in order to avoid any interference, and in addition, all the processes of measurement have been repeated another time.
From the elaboration of measurements, the characteristic curve of the system has been estimated for each case, as shown in figure 3. It is clear that the presence of the screens modifies the characteristic curve of the system, presented in the first image (black curve). On one hand, the presence of H4 and H5 respectively increases fluid velocity within the channel compared to the normal values, at the same fan frequency. This fact can be linked to the characteristic texture of these two screens. In fact, the flow is free to pass through the porous strips, which have the effect of accelerating the flow, reducing the passage area (Venturi effect). These porous parts are located at such a limited distance (2 or 3 strips of distance equal to 8-12 mm) to determine overall an higher air speed in the whole measurement section downstream of the screens. On the other hand, the results of screen H3 shows a different situation. As in the previous cases, this fact is due to the screen's texture, which blocks the fluid passage, as an obstacle, in this case. The H3 texture is composed of strips of plastic, totally without porous strips that allow air to pass through and only with minimal fissures between strips, which stops the flow of air, causing the air velocity decrease recorded in the measurements. After this first phase, measurements of pressure have been conducted by placing the tubes of the instrument before and after the sample in order to obtain a pressure drop (Δp) value. In this way, it will be possible to define the relation between air velocity and pressure drop, refereed to each case.

3.3. ***Images elaboration***

The porosity of a screen is strictly linked to its permeability and inertial coefficient factor, as shown in section 1 (eq. 5, 6, 7).

However, for this type of screens the porosity is usually not available as it is not easy to obtain. For these reasons the porosity has been evaluated by means of image analyses within Matlab environment. First of all, each screen has been scanned by an Epson Scannerjet 5530, with an optical resolution of 2400 $\times$ 4800 dpi. In this case, a resolution of 1200 dpi has been chosen. Considering the limited area that the scan could analyze and the observed repetitiveness of the texture, three portions of the whole sample have been considered and

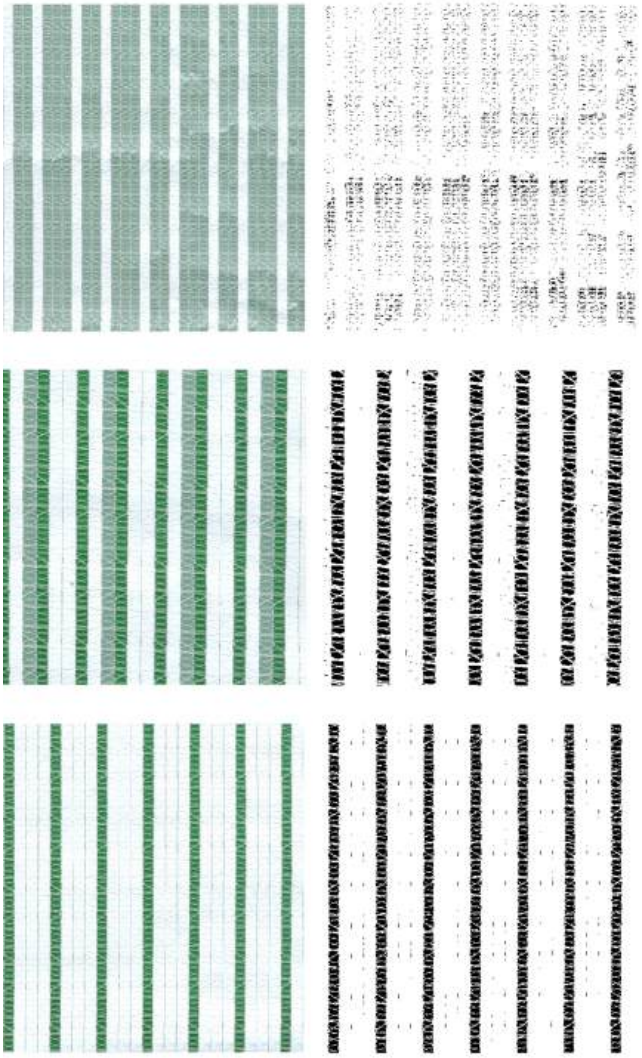

Figure 4: Figure representing the comparison of the scanned sample and the Matlab manipulation result. From the top there are: H3, H4 and H5.

scanned, as characterization of the entire sample. The porosity of the screens has been obtained by a Matlab analysis described as follows. The raw image has been converted in a "black and white" one by means of the Matlab tools rgb2gray and im2bw. Figure 4 shows the starting images for the three screens on the left column and the manipulated ones on the right column. The ratio between the number of black pixels and the total number of pixels in the "black and white" figure gives the ratio between empty spaces and the total area occupied by the screen, *i.e.* the porosity of the screen.

3.4. ***CFD approaches and grid convergence***

For the CFD approach, the H5 has been modeled as study case with two different approaches. A scaled model of 3 $\times$ 3 cm has been created using Autodesk Inventor. The model, for the CFD approach (1) has been created

drawing a central portion of the scanned sample, emblematic of its structure, and the dimension of the total domain is 3 × 3 × 18 cm, as shown in fig. 5. For the CFD approach (2), the full screen has been modeled as a porous surface with the characteristics experimentally defined, in a domain of 30 × 30 × 180 cm. The meshing process has been performed using ICEM CFD and the simulations have been conducted using Ansys-inc Fluent 17.2. The meshes are unstructured meshes of tetrahedral elements for both the approaches, obtained by the application of Robust (Octree) method. The turbulence model used is a standard k-epsilon model.

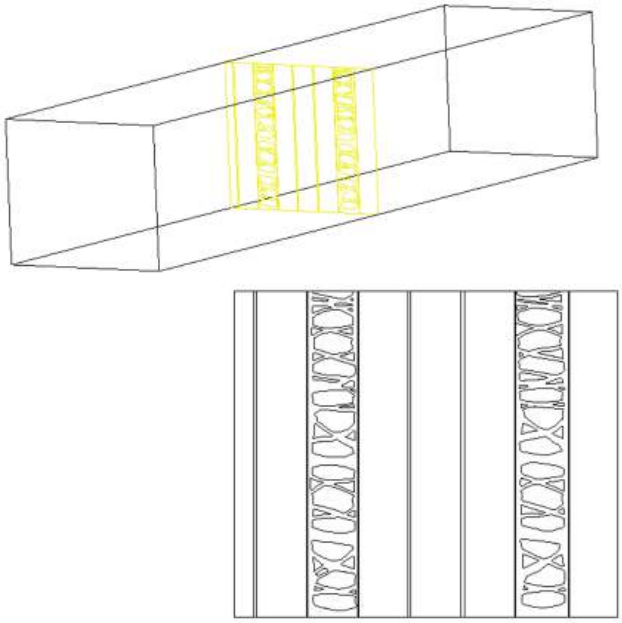

Figure 5: 3D model of the entire domain (at left) and a zoom of screen modeling (at right), of the CFD approach (1)

.

The figure 6 shows the unstructured mesh of the screen, in approach (1). The porous areas have been modeled as an interior surface where the air could flow freely and the stripes and thread as walls, impermeable to the fluid passage. The lateral surfaces have been defined as symmetries. Figure 6 shows that also the tiny fissures between the stripes have been modeled as open surfaces. The sample has been considered as a surface, based on its tiny thickness.

Seven different meshes have been performed, with different refinement of grids, from 3×10^5 to 1.4×10^7 cells, for the grid sensitivity study of the approach (1). Five meshes have been carried out for the approach (2).

The comparison for the approach (1) has been conducted among twelve different velocity profiles, considering three profiles in four different distances from the screen surface. In specific, the sections chosen have been placed at 3 and 6 cm from the screen, in both directions. In approach (2) eight different velocity profiles have been taken in account for the comparison, considering

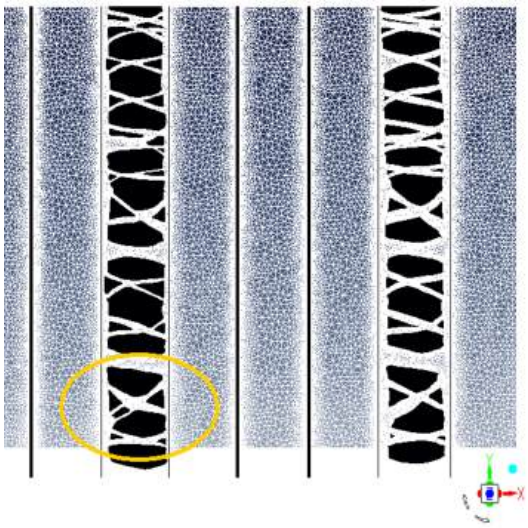

Figure 6: The figure shows an image of the mesh of the screen.

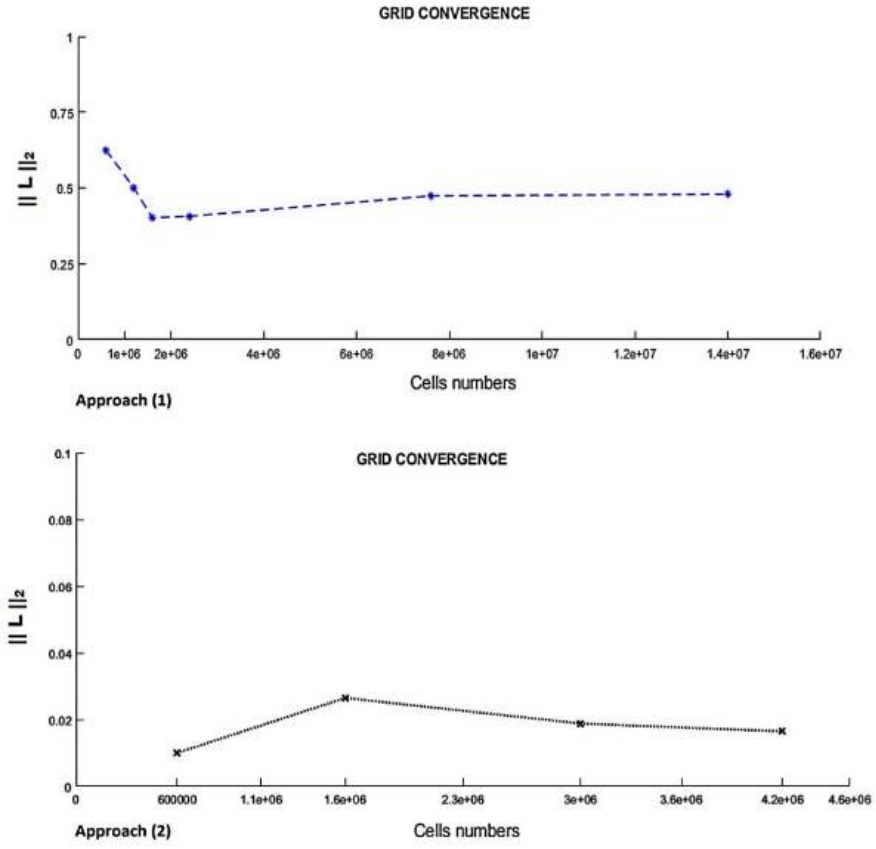

Figure 7: Results of the grid convergence study for both approaches, calculating the $\|L\|_2$ of several velocity profiles, coming from each simulation.

four profiles in two different sections. These sections have been defined at 30 cm before and after the screen. The same methodology has been used as

described as follows. The $\|L\|_2$ norm has been calculated between the profiles of two different grids, starting from the coarsest to the finest one. The results have been reported in figure 7. It is visible that the stabilized trend of simulation results , for the approach (1), is obtained between the fifth mesh and the seventh one, which leads to choose the sixth mesh (7.6×10^6 with cells dimensions for the screens of the order of 10^{-2}mm). Instead, the trend of the results for the approach (2) is quite stable since the first value. 3×10^6 of cells mesh has been chosen for the simulations and convergence criteria of 10^{-5} for continuity and 10^{-6} for all other parameters have been chosen for convergence achievement.

3.5. ***PIV measurements***

In order to validate the CFD model and evaluate the realistic modeling of the phenomenon, on a physical point of view, by the CFD approach, Particle Image Velocimetry (PIV) measurements in wind tunnel have been performed.

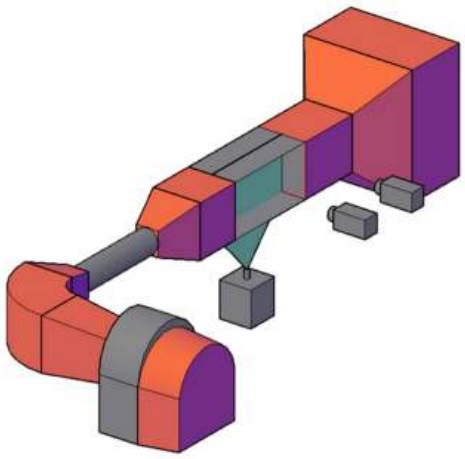

Figure 8: Image represents a simplified scheme of PIV set up, with cameras and laser layer visible in the test room.

In this paper, this technique has been performed to study the effect of the screens, seen as an obstacle, on the air flow. In this case, the H5 has been placed inside the test chamber. The PIV setup consists of a Dantec Dynamics System with two cameras Flowsense M2/E with Nikon lenses AF micro-Niccor 60 mm, a New Wave Research Laser with a cylindrical lens to produce a laser sheet, a synchronizing system for triggering the image acquisition with the laser shots. The air-flow within the wind-tunnel has been seeded by micro oil particles produced by a smoke machine (Jem Techno-Fog). Flow-Manager v. 4.71 software has been used for the post-processing of the optical images. Two cameras are usually used simultaneously in order to obtain a 3D particle image velocimetry; in this case, the experiments have been conducted in 2D with both cameras for observing simultaneously the out-coming flow, close to

the sample and the flow at the outlet of the test chamber. A set of 40 couples of images has been recorder for each measurement. Each couple of images records the positions of the oil-particles in two very near time-instants (Dt=400 μs for the case shown in this section). From each couple of images, a raw velocity map has been obtained by means of cross-correlation procedure that yields the average velocity of the particles contained in small subdivisions of the images. The ensemble of all the velocity vectors obtained gives the raw velocity map correspondent to the time interval Dt.

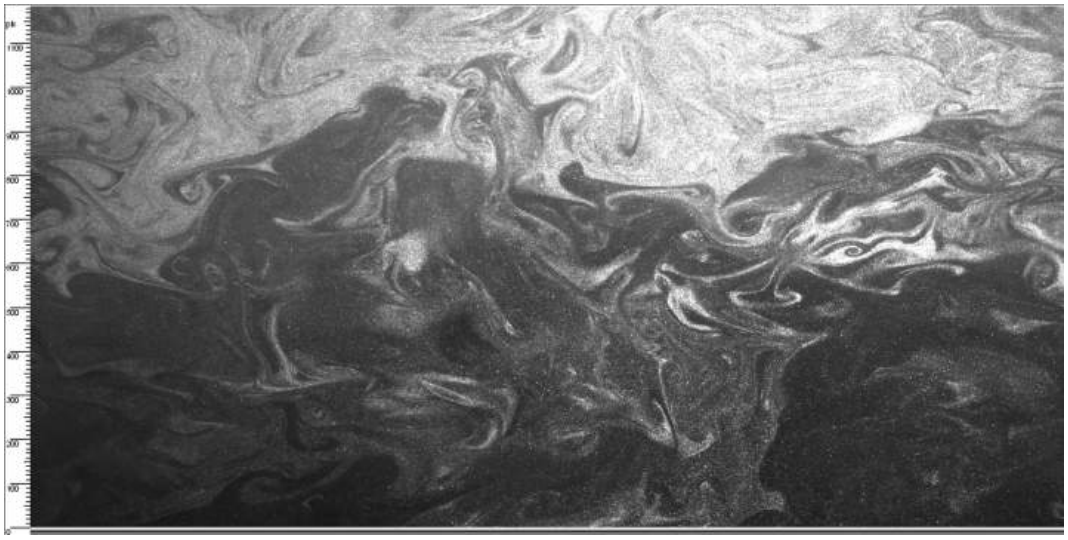

Figure 9: Example of a picture watchable in a PIV experiments. In specific, this is obtained during the test conducted with the sample of screen H5.

In order to compare PIV results with CFD velocity distributions, an average of a number of instantaneous experimental velocity maps is needed. The fan frequency has been set at 10 Hz that corresponds to a 1 m/s of air velocity. Examples of pictures obtainable from the measurements are showed in figure 9. The results consisted in 40 raw velocity vector maps representative of the air flow velocity, which have been analyzed by moving average filter. After this process, the data have been elaborated also through Matlab, in order to obtain averaged velocity values from the instantaneous results coming from the PIV measurements. In particular, from each image an average of the phenomenon has been obtained by calculating the mean values of each profile present in every picture, within every image obtained in the test. This results should be comparable with the CFD results, considering them a average values of the flow.

4. Results and Discussion

In this section, the results of the two approaches for screens characterization presented in the previous sections are shown. The first approach (totally

experimental) is the combination of wind tunnel tests and image process analysis. The second approach is a CFD approach based on a validation by means of PIV measurements.

4.1. ***Results of the experimental approach***

The pressure data obtained from measurements have been related to the air velocity, in order to obtain the following relations in figure 10.

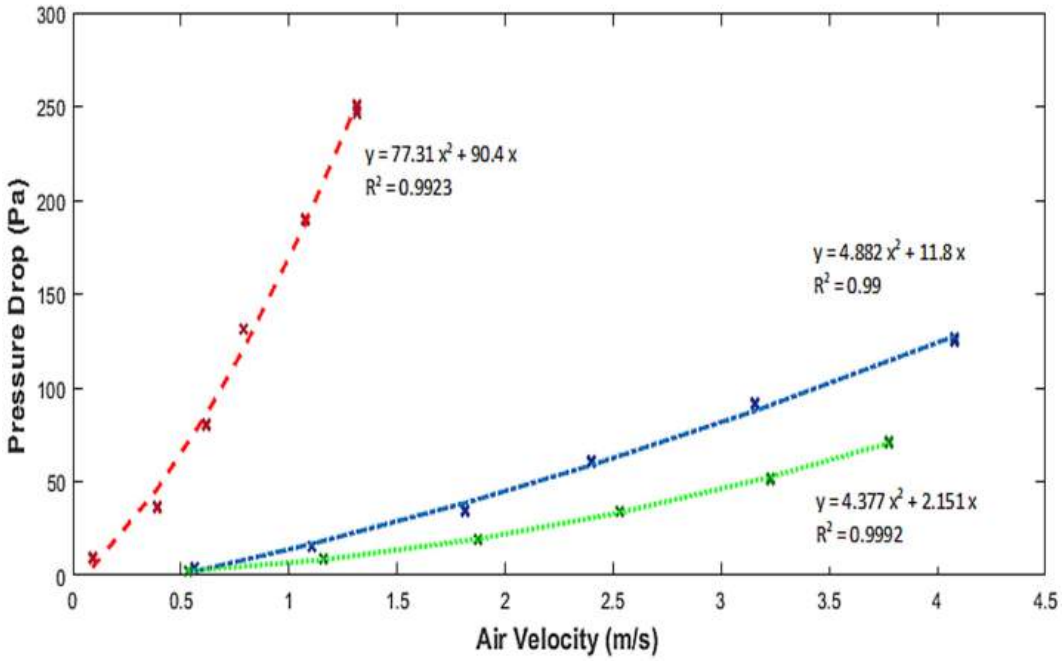

Figure 10: Characteristic curve of screens: red curve refers to H3, green curve refers to H4 and blue one to H5.

It is clear in fig. 10 that the screens differently affect the air flow due to the texture differences. Considering the fitting results, the screens H4 and H5 have a more similar trend and coefficients of the equations. Moreover, it is recognizable when there is only the contribution of Darcy's term (linear part) and when there is also the contribution of Forchheimer's term (parabolic profile). In fact, similar pressures have been recorded during the measurements with the progressive increase of air velocity. By substituting the coefficients of the fitting equations (shown in figure 10) in equations eq. (3), it is possible to obtain the permeability K and the inertial factor Y, as:

$$K = \frac{\Delta x \mu}{b} \tag{8}$$

$$Y = \frac{a\sqrt{K}}{\Delta x \times \rho} \tag{9}$$

where ρ is 1.225 (kg/m^3), μ is 1,81 $\times$ 10^{-5} (Pa s) and Δx is the thickness of samples, which has been measured by a mechanical feeler. The results of the data elaborations and calculations have been summarized in table 2.

Table 2: Data obtained from the elaborations of data collected in experiments and parameters calculated.

	a	b	Δx	Y	K
H4	4.377	2.151	0.00032m	0.5794	2.6627×10^{-9}
H5	4.882	11.8	0.00032m	0.2759	$4{,}9085 \times 10^{-10}$
H3	77.31	90.4	0.00036m	1.4883	7.2080×10^{-11}

These results outline the fact that the permeability values differ from each other by an order of magnitude. Despite the permeability tends to decrease with the opening spaces reduction, the inertial coefficient does not increase according to the same trend. It is possible to observe that the porosity has the same trend of the permeability, as outlined for the data in table 2. Then, the permeability is strictly dependent on porosity, as expected.

4.2. ***Measurements of porosity***

By following the process explained in section 2.3, the porosity of the three samples has been evaluated and presented in table 3.

Table 3: Results of image analysis of screen samples, with each single value obtained and the average of them.

	1	2	3	average	standard deviation
H4	0.2133	0.2076	0.20	0.2070	$\pm$0.0067
H5	0.1727	0.1635	0.1639	0.1667	$\pm$0.0052
H3	0.0338	0.0294	0.0273	0.0302	$\pm$0.0033

The standard deviation values show a small uncertainty, about 3%, in the porosity evaluation of cases H4 and H5; instead, the standard deviation is about 10% in case H3.

In order to find the right correlation for the types of screens analyzed in this paper, the relations between porosity and permeability, such as between porosity and inertial coefficient have been investigated, in analogy with equations (5), (6) and (7). From experimental porosity and permeability, the correlation shown in Figure 11 has being obtained. Comparing this result with the relations available in the literature (Miguel, 1998) a very good agreement with a parabolic trend is shown.

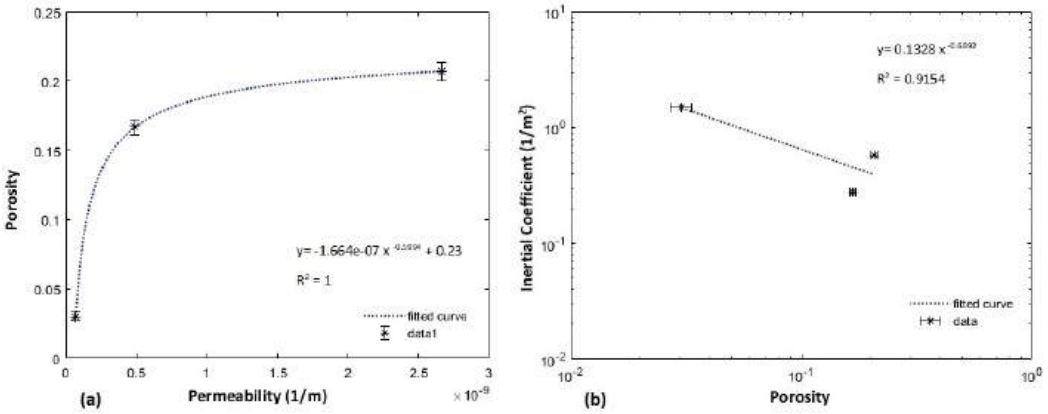

Figure 11: The curve fitting of porosity and permeability **(a)** is presented at left and porosity and inertial coefficient **(b)** at right.

In analogy to the permeability, the fitting relation of experimental data of porosity and inertial coefficient has been presented in Figure 11 and the relative correlation has been obtained. In particular, the resulting equations have this form:

$$\alpha = a \times K^b + c \tag{10}$$

$$Y = d \times \alpha^e \tag{11}$$

where a, b, c, d, e are coefficients derived form the fitting of the data.

It can be observed that the zero order term can be neglected with respect to the higher order terms. Then, the final equations of the inertial coefficient (eq. 12) and permeability (eq. 13) can be carried out.

$$Y = 0.1328 \times \alpha^{-0.6892} \tag{12}$$

$$K = 1.664 \times 10^{-7} \alpha^{-1.6683} \tag{13}$$

The model equations for these type of screens are completely analogous to the ones elaborated in the works by (Miguel, 1998; Valera et al., 2005).

4.3. ***Results of the CFD-PIV approach***

In the PIV measurements, two areas have been analyzed: one is immediately downstream in fig. 12 of the screen and the other one is the section at a distance of about 20 cm from the screen in fig. 13, where the flow should be less affected by the perturbation given by the screen presence. Figures 12 and 13 shows the PIV results for the two positions, where the air flow comes from right.

The top images in the fig. 12 and the fig. 13 show the instantaneous picture of oil particles at two specific positions. The right image shows the high density of oil particles streams crossing the empty strips of the screen. The left image

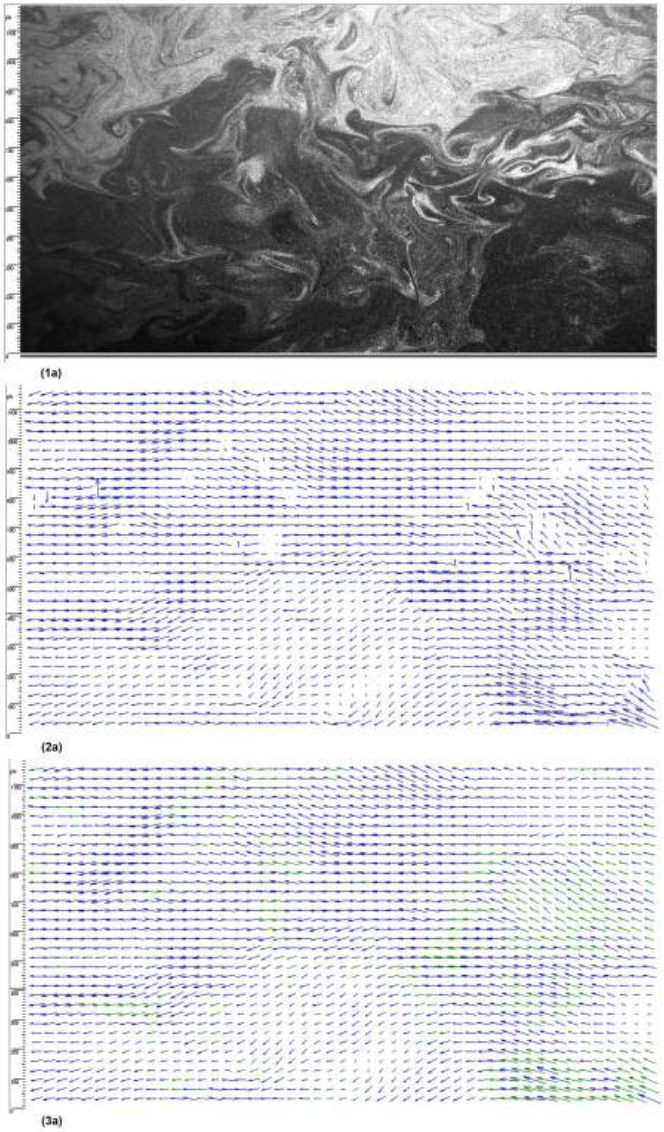

Figure 12: In this figure are presented the raw vector maps (central line) and the maps resulting from the moving average method (bottom line), related to the images in the top line.

shows a high recirculating flow. The second line in the figures 12 and 13 show the raw velocity vector maps obtained from the PIV technique. The third line presents the vector maps obtained by a moving average filter (Smith, 1999). The raw vector maps and the results of the moving average method are shown in figures 12 and 13. The green vectors in this figure represent the filtered vectors. These results shows that near the screen is necessary to filter larger areas as it is a region characterized by re-circulation between two jet flows. On the other hand, far from the screen, the average motion of the air particular is more regular and less filtering is needed. To choose the appropriate boundary conditions for the CFD simulations, a preliminary analysis has been performed on these PIV velocity maps in zones having the same dimensions as the portions

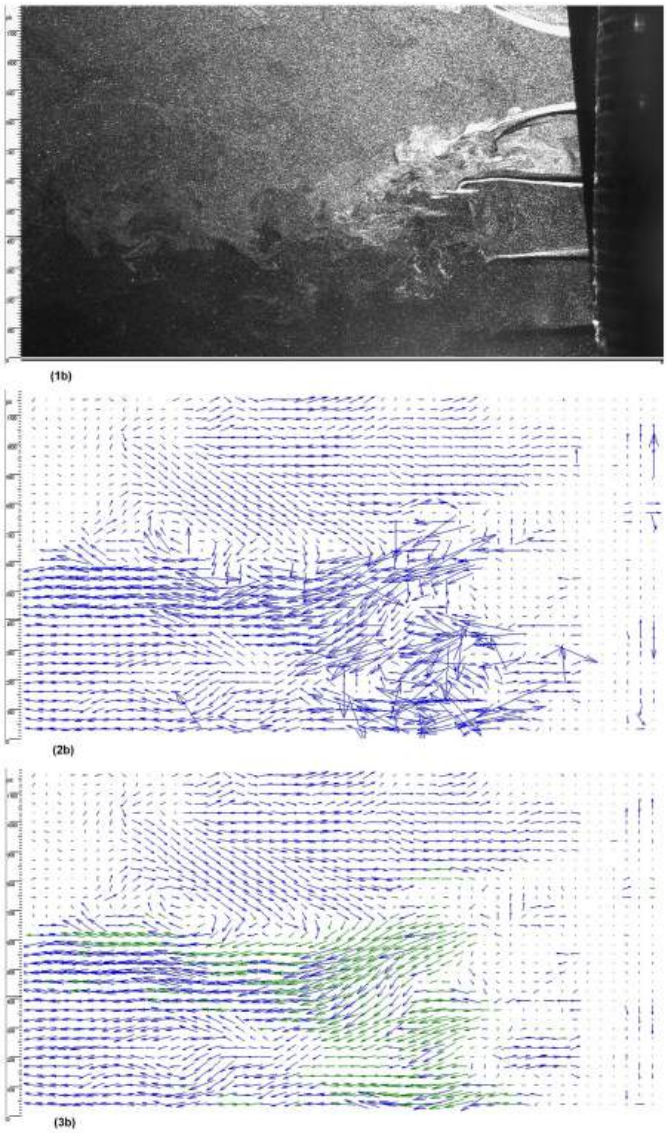

Figure 13: In this figure are presented the raw vector maps (central line) and the maps resulting from the moving average method (bottom line), related to the images in the top line.

of the screen considered for the CFD analysis and shown by figure 5. Taking an average of 40 measurements, the velocities of 0.34 m/s and 0.65 m/s have been obtained in correspondence of 5 and 10 Hz respectively. These velocities have been used as inlet velocities in the CFD simulation of the small model of the screen.

The comparison between the static pressures obtained for these two cases with approach (1) are shown in table 4.The table 4 shows a very good agreement between simulated and measured data for the ~~two cases analyzed~~ the approach (1), as the relative errors are 8.3 % and to the 0.6 % respectively. In the second approach, results are significantly different from the PIV measurement data.

Table 4: Values of pressure drops measured and simulated, caused by the presence of the screens for the approach (1).

	5 Hz	10 Hz
Measurements	4.13	15.48
CFD approach (1)	4.55	15.3
Error	8.3 %	0.6 %

In the second approach, the velocity used as initial boundary condition is the air velocity collected in the wind tunnel tests for a fan frequency of 10 Hz. These magnitude velocity is 1.1 m/s. In analogy to the first approach results, in table 5 the comparison between measured pressures and simulated once is presented.

Table 5: Values of pressure drops measured and simulated, caused by the presence of the screens for the approach (2).

	10 Hz
Measurements	15.48
CFD approach (2)	15.6
Error	0.8%

The results, shown in table 5, present considerably limited differences between the measured data and the simulated one, with an error of 0.8%.Then, a negligible overestimation of the pressure drop of the air flow through the screen can occur applying the CFD approach(2). The CFD velocity maps obtained from the two CFD modeling approaches have been compared with the ones obtained by PIV measurements, in position x_1 and x_2. The vector map obtained from the middle section of the CFD model (1) (top) is shown in fig.14 and compared with the velocity map obtained by PIV measurements (bottom). The vector map obtained from the middle section of the CFD model (2)(top) is shown in fig. 15 and compared with the velocity map obtained by PIV measurements (bottom).

In the first case, the CFD velocity map shows two symmetrical counter rotating vortices between the two jets. Similar vortices are observed in PIV velocity map. In this case, the vortices are smaller and not symmetrical, as the PIV results correspond to a limited time interval. The CFD results present a good agreement with the PIV measurements.

In the second case, the vector maps are sensibly different. In fact, if the screen is modeled as a porous surface, no vortices are obtained. The air flow distribution does not present any visible turbulence effect. The presence of the screen slightly block the air flow, so decreasing his magnitude. However,

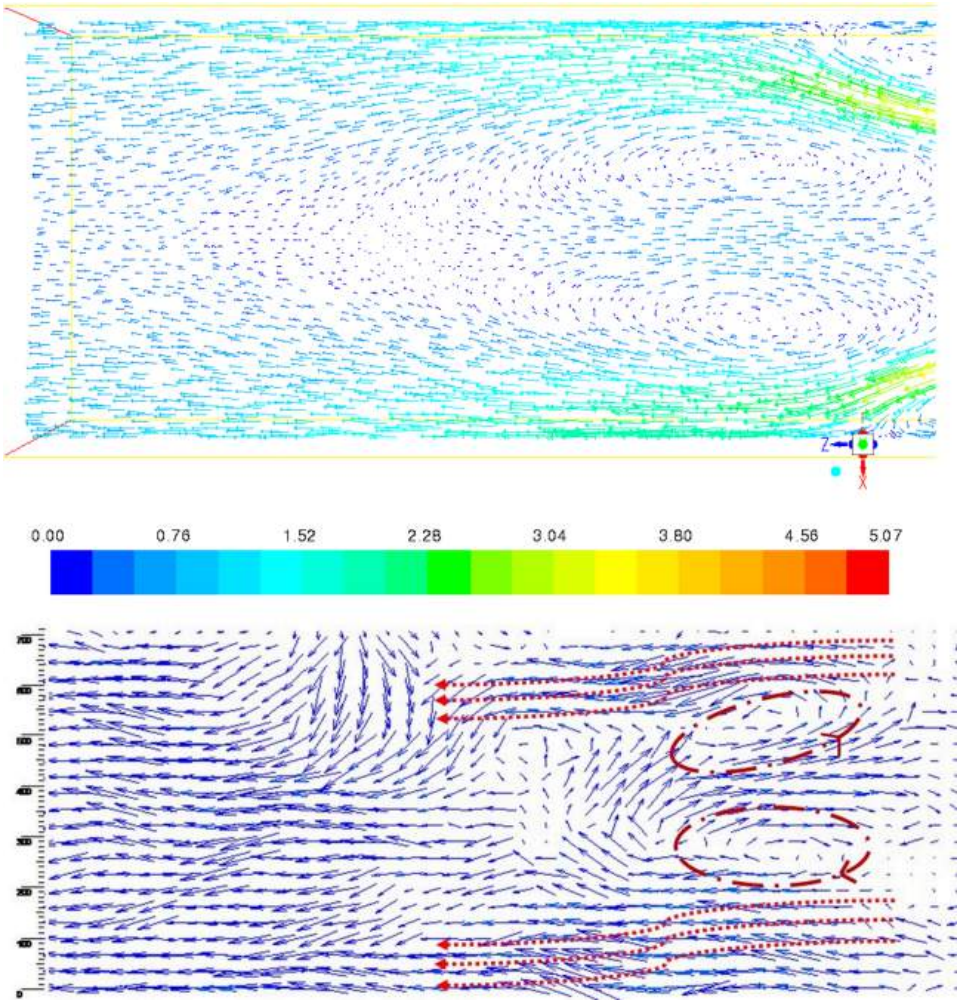

Figure 14: In the upper part a vector map, obtained from the simulation with initial air velocity of 0.6 m/s, is reported with below the vector map resulting from PIV measurement.

the results of the PIV measurements clearly showed presence of vortices just downstream of the screen.

The porous surface approach can describe accurately the air flow through a screen in terms of air velocity magnitude and pressure. However, through this approach the local distribution of flow structures as vortices, due to the texture and geometrical characteristics of a screen, cannot be obtained. Despite this, the CFD results have shown a significant consistency and accuracy with the measurements obtained by the PIV, under different point of views. The CFD model in small scale has proved to be a good tool to investigate the fluid-dynamics of the air passage through a complex texture screen. The porous surface approach has proved to be applicable for modeling the fluid dynamic through a screen, considering its effects on a bigger system, for example in a greenhouse or any other building, where the effects given by the details of the screen texture can be neglected.

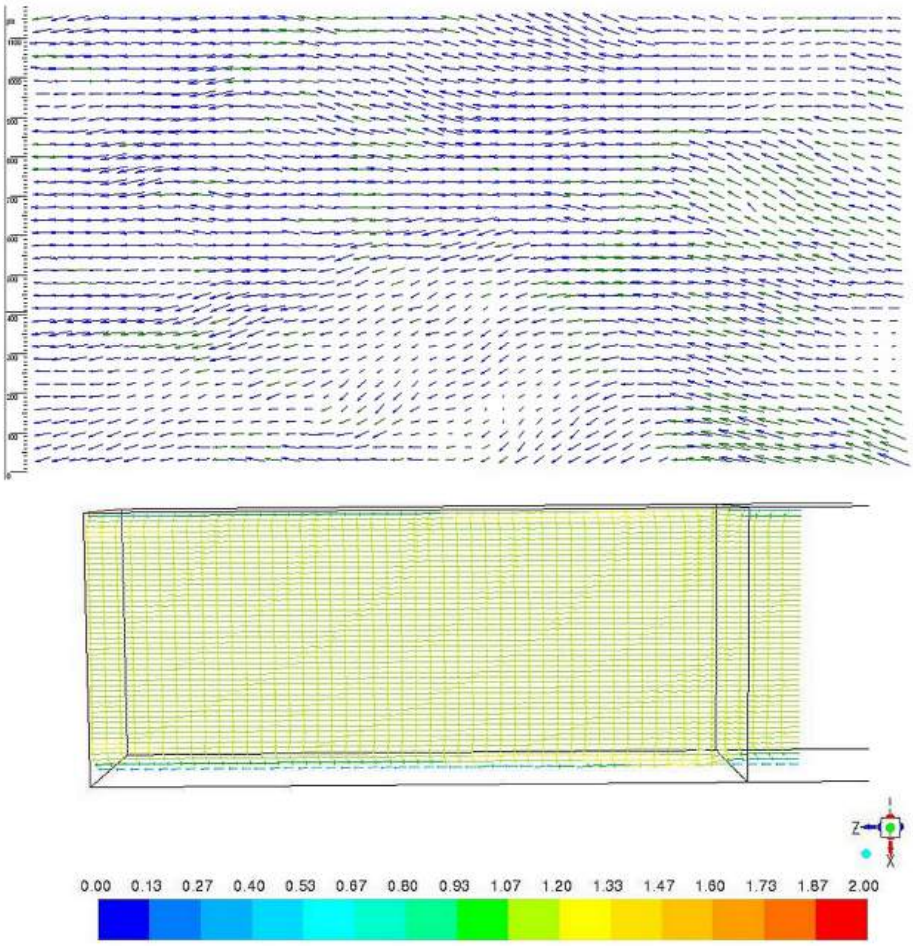

Figure 15: In the upper part a vector map of the simulation with approach (2) is reported with below the vector map resulting from PIV measurement.

5. Conclusions

It is well known that shading screens used in greenhouses can significantly affect the air flow patterns inside the structure. However, previous studies are mainly focused on types of screens with a regular texture, whereas new types of shading screens with more complex textures now available on the market are becoming more and more commonly used in the protected cultivation sector For these screens, no methodology is available for their characterization. New methodologies for the characterization of the properties of complex-texture screens thus need to be defined and validated. This study stemmed from this need of advancement of knowledge in the greenhouse sector, focusing on an experimental approach and a combined experimental and numerical methodology that have been designed and tested and evaluated.

A novel approach based on image analysis together with wind tunnel tests has been set up to yield the permeability and inertial coefficient. In particular, several types of shading screens have been analyzed and experimentally

characterized by means of wind tunnel tests: air velocity and pressure drop measurements have allowed to define the specific behavior of each screen, which proves fundamental to investigate the specific effects of shading screens on air flows in greenhouses. By this approach, the proper mathematical correlation for the new kind of screens considered in this paper has been found.
On the other hand, a computational methodology based on CFD modeling has been carried out in order to obtain the relation between air velocity through a screen and the relative pressure drop, avoiding any experiment. The air velocity fields obtained from CFD simulations have been validated by means a comparison with velocity maps obtained experimentally from PIV measurements. This novel combined experimental-numerical approach gives information on the local dynamics of air between screen treads and strips. The proposed CFD application allows to provide a description of the fluid-dynamics phenomena which is consistent with the results obtained by means of Particle Image Velocimetry, used as golden standard. Both the two methodologies shown in this paper allow to obtain the parameters necessary to investigate the screens effects on the ventilation and on the indoor climatic conditions of a greenhouse.

References

References

T Bartzanas, T Boulard, and C Kittas. Numerical simulation of the airflow and temperature distribution in a tunnel greenhouse equipped with insect-proof screen in the openings. *Computers and Electronics in Agriculture*, 34: 207–221, 2002.

J. B. Campen. Greenhouse design applying CFD for Indonesian conditions. *Acta Horticulturae*, 691:605–614, 2005.

J. B. Campen and G. P.A. Bot. Determination of greenhouse-specific aspects of ventilation using three-dimensional computational fluid dynamics. *Biosystems Engineering*, 84:69–77, 2003.

S. Castellano, Scarascia G. Mugnozza, G. Russo, D. Briassoulis, A. Mistriotis, S. Hemming, and D. Waaijenberg. Design and use criteria of netting systems for agricultural production in italy. *Journal of Agricultural Engineering*, 3: 31–42, 2009.

U. M. S. Costa, J. S. Andrade, H. A. Makse, and H. E. Stanley. Inertial Effects on Fluid Flow through Disordered Porous Media. *Physica A: Statistical Mechanics and its Applications*, 266(1-4):420–424, sep 1998.

R. E. Ewing, R. D. Lazarov, S. L. Lyons, Dimitrios V. Papavassiliou, J. Pasciak, and G. Qin. Numerical well model for non-darcy flow through isotropic porous media.

Enrico Fabrizio. Energy reduction measures in agricultural greenhouses heating: Envelope, systems and solar energy collection. *Energy and Buildings*, 53:57 – 63, 2012. ISSN 0378-7788.

Hicham Fatnassi, Thierry Boulard, and Lahcen Bouirden. Simulation of climatic conditions in full-scale greenhouse fitted with insect-proof screens. *Agricultural and Forest Meteorology*, 118:97–111, 2003.

J. Flores-Velazquez and J.I Montero. Computational fluid dynamics (CFD) study of large scale screenhouses. *Acta Horticulturae*, 797:117–122, 2008.

J.G.I. Hellström and T.S. Lundtröm.

N. Katsoulas, T. Bartzanas, T. Boulard, M. Mermier, and C. Kittas. Effect of vent openings and insect screens on greenhouse ventilation. *Biosystems Engineering*, 93:427–436, 2006.

A. F. Miguel. Airflow through porous screens: From theory to practical considerations. *Energy and Buildings*, 28:63–69, 1998.

A. F. Miguel, N. J. Van De Braak, and G. P.A. Bot. Analysis of the airflow characteristics of greenhouse screening materials. *Journal of Agricultural and Engineering Research*, 67:105–112, 1997.

Francisco Domingo Molina-Aiz, Diego Luis Valera, and Antonio Jesús Álvarez. Measurement and simulation of climate inside Almeria-type greenhouses using computational fluid dynamics. *Agricultural and Forest Meteorology*, 125: 33–51, 2004.

D. Naylor, S. S. M. Foroushani, and D. Zalcman. Free convection heat transfer from a window glazing with an insect screen. *Energy & Buildings*, 138:206–214, 2017.

Neil Norris and Michael Collins. Modelling the effects of insect screens on natural convection in window cavities, 2015.

Enrica Santolini, Beatrice Pulvirenti, Stefano Benni, Luca Barbaresi, Daniele Torreggiani, and Patrizia Tassinari. Numerical study of wind-driven natural ventilation in a greenhouse with screens. *Computers and Electronics in Agriculture*, 149:41–53, 2018.

Steven W. Smith. The Scientist and Engineer's Guide to Digital Signal Processing. chapter 15, page 672. California Technical Publishing, 1999.

W. Sobieski and A. Trykozko. Darcy 's and forchheimer 's laws in practice . part 1 . the experiment. *Technical Sciences*, 17:321–335, 2014a.

W. Sobieski and A. Trykozko. Darcy's and forchheimer's laws in practice. part 2. the numerical model. *Technical Sciences*, 17:321–335, 2014b.

M. Teitel. Using computational fluid dynamics simulations to determine pressure drops on woven screens. *Biosystems Engineering*, 105:172–179, 2010.

M Teitel and A Shklyar. Pressure drop across insect-proof screens. *Transactions of the ASAE*, 41(6):1829–1834, 1998.

Meir Teitel. The effect of screened openings on greenhouse microclimate. *Agricultural and Forest Meteorology*, 143:159–175, 2007.

D. L. Valera, F. D. Molina, A. J. Álvarez, J. A. López, J. M. Terrés-Nicoli, and A. Madueño. Contribution to characterisation of insect-proof screens: Experimental measurements in wind tunnel and cfd simulation. *Acta Horticulturae*, 691:441–448, 2005.

D. L. Valera, A. J. Álvarez, and F. D. Molina. Aerodynamic analysis of several insect-proof screens used in greenhouses. *Spanish Journal of Agricultural Research*, 4:273–279, 2006.

G. Vox, I. Blanco, G. Scarascia Mugnozza, E. Schettini, C. Bibbiani, C. Viola, and C. A. Campiotti. Solar Absorption Cooling System for Greenhouse Climate Control: Technical Evaluation. In Son, JE and Lee, IB and Oh, MM, editor, *International Symposium on new Technologies For Environment Control, Energy-Saving and Crop Production in Greenhouse and Plant Factory-GREENSYS 2013*, volume 1037 of *Acta Horticulturae*, pages 533–538, 2014. ISBN 978-94-62610-24-8.

Guoqiang Zhang, Christopher Choi, Thomas Bartzanas, In-Bok Lee, and Murat Kacira. Computational fluid dynamics (cfd) research and application in agricultural and biological engineering. *Computers and Electronics in Agriculture*, 149:1 – 2, 2018.